Magic mode switching in Yb:CaGdAlO 4 laser under high pump power

Frédéric Druon, Mickaël Olivier, Anaël Jaffrès, Pascal Loiseau, Nicolas Aubry, Julien Didierjean, François Balembois, Bruno Viana, Patrick Georges

Magic mode switching in Yb:$CaGdAlO_4$ laser under high pump power

Frédéric Druon,[1,*] Mickaël Olivier,[1] Anaël Jaffrès,[2] Pascal Loiseau,[2] Nicolas Aubry,[3] Julien DidierJean,[3] François Balembois,[1] Bruno Viana,[2] and Patrick Georges[1]

[1]*Laboratoire Charles Fabry, Institut d'Optique, CNRS, Univ Paris Sud, 2 Avenue Augustin Fresnel, 91127 Palaiseau Cedex, France*

[2]*Chimie-Paristech, Laboratoire de Chimie de la Matière Condensée de Paris, CNRS-UMR 7574, UPMC Univ Paris 06, 11 rue Pierre et Marie Curie, 75005 Paris, France*

[3]*Fibercryst S.A.S., Parc d'Activités Wilson—Bat A1, 31 rue Wilson, 69150 Decines Charpieu, France*

**Corresponding author: frederic.druon@institutoptique.fr*

We present unique spatial-mode switching in a cw Yb:CALGO laser when pumped at a multihundred-watts power level. It permits us to automatically stabilize to a TEM_{00} mode from a highly spatial multimode regime. This stabilization is achievable thanks to polarization-mode switching allowed by the particular spectroscopic and thermal properties of Yb:CALGO crystal. This atypical and unexpected behavior is studied in detail in this Letter and explained by analysis of the thermo-optical coefficients for CALGO.

Diode-pumped high-power lasers based on Yb-doped materials have raised intense interest in the laser community in the last few years. Among them, Yb-doped $CaGdAlO_4$ crystal (Yb:CALGO) is now recognized to exhibit exceptional and interesting properties for high-power and ultra-short-pulse lasers. In fact, by combining both broad emission bandwidth and good thermal properties, it permits us to demonstrate ultra-short pulses [1,2] and high power [3–6]. Very recently, this crystal also has been integrated in thin-disk geometry [7,8], demonstrating in cw up to 150 W (multimode) and 50 W (single mode) and up to 30 W in femtosecond regime [9]. These experiments clearly demonstrate the interest of Yb:CALGO in classical bulk or thin-disk configurations for high-power femtosecond lasers.

Increasing the pump power (typically > 100 W), the thermal issues start to be problematic in Yb:CALGO. Nevertheless, the analysis of the thermal lens in CALGO has never been carried out in detail up to now. Indeed, very few thermal parameters are known for Yb:CALGO. In this Letter, the thermal properties are studied carefully in order to explain an unexpected and, to our best knowledge, never-observed-before effect consisting of a drastic spatial mode stabilization by passive polarization switching.

The laser cavity is shown in Fig. 1. It is a three-mirror V-shape cavity incorporating a plane dichroic mirror, a 500 mm radius-of-curvature mirror and a plane mirror as the output coupler. The Yb:CALGO is a 10 mm long 2 at. %-doped crystal with a section of 2×2 mm^2. The crystal is pumped with a 400 μm diameter fiber-coupled (NA = 0.22) diode delivering up to 200 W. The diode beam is imaged in the crystal with a magnification of 1.

In this configuration, the crystal absorbs between 90% (at low power) and 75% (at high power) of the pump power, depending on the absorption saturation. The optimal output coupler transmission is 10%, allowing extraction of cw power up to 43 W. The crystal is integrated in a copper mount, which is water cooled at 18°C. This module design, based on Taranis technology from Fibercryst, is used to optimize the heat-transfer coefficient and minimize mechanical stresses. The temperature elevation, measured with an IR 8 to 12 μm camera, at the entrance surface and in the center of the crystal is 0.66 K/W (versus absorbed power), which leads to a 100 K increase at full power.

Experimentally, we observe a spatial single-mode operation at "low" pump power, typically under 88 W of absorbed pump power (100 W incident). Multimode operation, due to thermal lens effects, appears above this value. Surprisingly, the spatial mode switches back abruptly to a nice TEM_{00} mode when the pump reaches 128 W of absorbed pump power (160 W incident) as shown in Fig. 2. Increasing furthermore the pump power, the spatial mode does not degrade back to highly multimode operation but stays almost TEM_{00} with only a slight astigmatism and a small amount of TEM_{20} (Fig. 2). We then observe a very different behavior before and after the switch.

We investigated the spectral and thermal properties of Yb:CALGO in order to understand this *magic* mode switching.

The first noticeable difference between the two laser beams before and after the switch is the polarization state. Actually, the linear polarization switches from vertical to horizontal. This corresponds with our crystal cut to a switch from a σ polarization ($E||\vec{a}$) to a π-polarization ($E||\vec{c}$), see Fig. 1. Since these two axes have different gain cross sections (Fig. 3), the emission wavelength switches

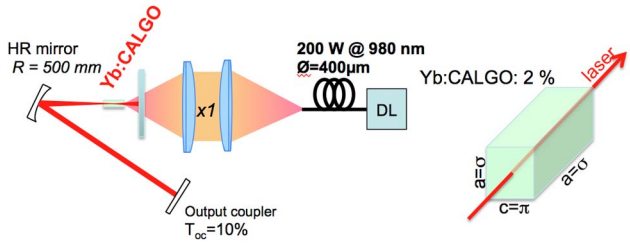

Fig. 1. Laser cavity (left). Crystal geometry (right).

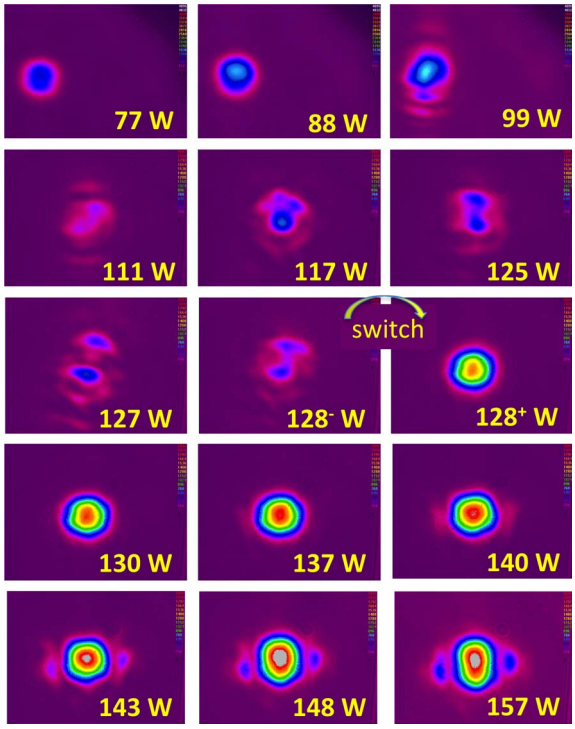

Fig. 2. Beam profile evolution versus absorbed pump power.

from 1047 to 1036 nm, which corresponds to the emission wavelength peaks, taking into account the reabsorption and the inversion population ratio (Fig. 3, top). For the setup described in Fig. 1, the inversion population can be estimated around $\beta \approx 0.08$, which leads to a gain of 1.2 for

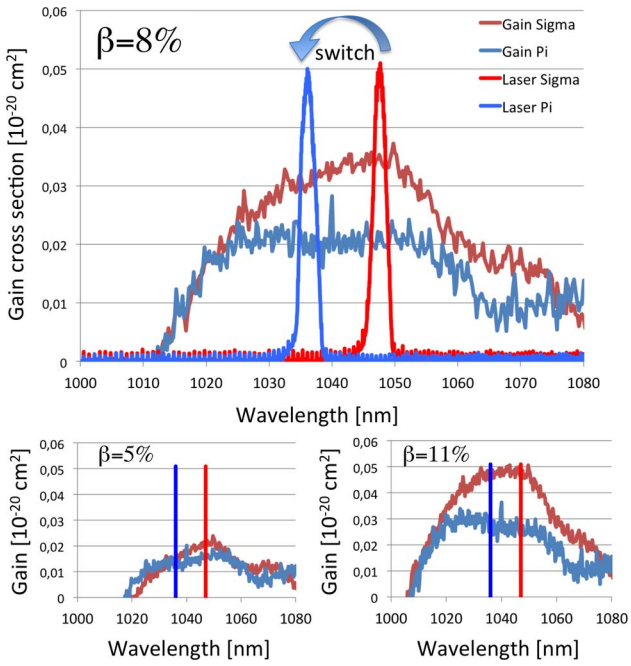

Fig. 3. (Top) Wavelength laser switching compared to the gain cross-section spectra (σ = red, π = blue) for a $\beta = 8\%$ (corresponding to the $T_{oc} = 10\%$). (Bottom) Gain cross sections for different population inversions demonstrating the increase, with β, of the gain difference between the two polarizations σ and π: examples taken for a $\beta = 5\%$ (corresponding to the $T_{oc} = 5\%$) and for a $\beta = 11\%$ (corresponding to the $T_{oc} = 15\%$).

the σ polarization and 1.12 for the π polarization. The cavity then has to have more losses for σ polarization than for the π polarization in order to authorize the switch.

This switch level also varies versus the inversion population and, consequently, versus the output couplers. Indeed, we observe the switch at 107, 118, 128, and 133 W of absorbed power for, respectively, 5, 8, 10, and 15% transmission output couplers, and the mode switch is not accessible with a 20% transmission output coupler. The particular spectroscopy of the Yb:CALGO can explain these variations in a level of polarization switching (Fig. 3, bottom). In fact, the higher the output coupler, the higher the gain and the inversion population (or equivalently β) are. This leads to the necessity of a bigger thermal lens to destabilize the σ polarized laser in favor of the π polarized laser because of the gain cross-section gap increase between the two polarization increases (Fig. 3).

As a consequence of the switch in emission wavelengths, the quantum defect also changes from 6.4% down to 5.4%, but only for the laser part [10]. Assuming a standard 2% of nonradiative decay and a fluorescence amount of four-fifths of the total radiative emission [11], the thermal loads for 128 W of absorbed power drops only from 6.3 W down to 6 W when switching from 1047 to 1036 nm. This drop is too small to explain the drastic spatial-mode modification. The answer to the mode switching, then, has to be found also by a study of the thermo-optic properties in CALGO.

To investigate the thermo-optic coefficient of CALGO, we measure the thermal wavefront distortions [12,13] using a wavefront sensor based on lateral shearing interferometry (SID 4 from Phasics). We analyze these distortions versus the probe polarization state (linearly polarized). The probe wavelength is 1030 nm. The pump beam is fiber-coupled and provides an unpolarized beam with a perfectly circular spatial beam profile.

The wavefront radius of the curvature in absolute value versus the probe polarization state is plotted in Fig. 4 for the two principal axes ($\vec{a}$ and $\vec{c}$) of the crystal for 128 W of absorbed pump power. First, one can observe a strong ellipticity, which means that the wavefront distortion depends on the probe polarization. Moreover, one may also observe a difference of these ellipticities depending on which axes of the crystal this wavefront is measured. This indicates a change in astigmatism of the thermal lens versus the polarization probe. This can be clearly observed in Fig. 5 representing the wavefront images taken for the two natural polarization axes σ and π.

This multidimensional variation can be explained by the role of the anisotropy of temperature-dependent refractive index, thermal expansion coefficients, and photoelastic effect [12–17]. Actually, the thermal expansion coefficients in CALGO are relatively different along the crystallographic axes: 10.1×10^{-6} K^{-1} along $\vec{a}$ and 16.2×10^{-6} K^{-1} along $\vec{c}$ whereas the thermal conductivity is almost isotropic: 6.9 Wm^{-1} K^{-1} along $\vec{a}$ and 6.3 Wm^{-1} K^{-1} along $\vec{c}$ (values given for a 2-% doped crystal).

From the point of view of the thermal lens (Fig. 6), for a polarization along the σ axis, the lens value is strong but

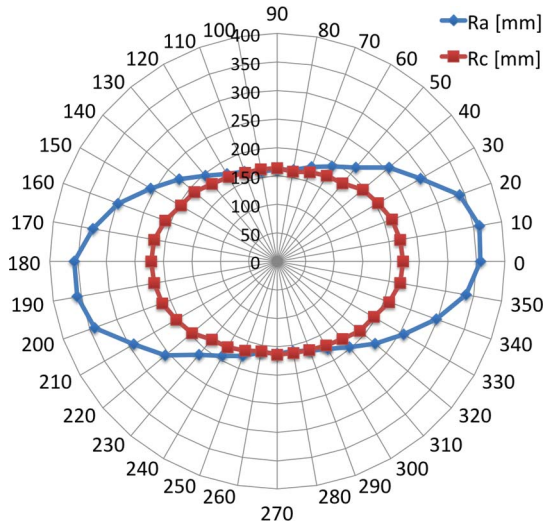

Fig. 4. Wavefront distortion analysis. Radius of curvature versus polarization of the probe (linearly polarized). 0° corresponds to a π-polarized probe and 90° to a σ-polarized probe. Two radii of curvature are measured along the principal axes of the crystal *id est* $\vec{a}$ and $\vec{c}$.

purely spherical (corresponding to the abscise values equal to 90°[180°] in Figs. 4 and 6). On the opposite, for a polarization along the π axis, the thermal lens is reduced, but a strong astigmatism appears (0°[180°] in Figs. 4 and 6). In Fig. 6, the astigmatism is defined as the difference between the dioptric powers along the two principal axes divided by the mean dioptric power. For probe polarization in between, the wavefront distortion does not depend on the polarization state of the probe at the output of the crystal. It only depends on the amount of the electric field projected on each crystallographic axis and not on the phase between these two projected components.

From these results on thermal lens properties of CALGO (Fig. 6), one can deduce the dioptry and the astigmatism of the lens, both versus the polarization beam propagating in the medium. One can notice that the axes of this astigmatic lens do not rotate with the polarization: the axes stay the same and correspond to

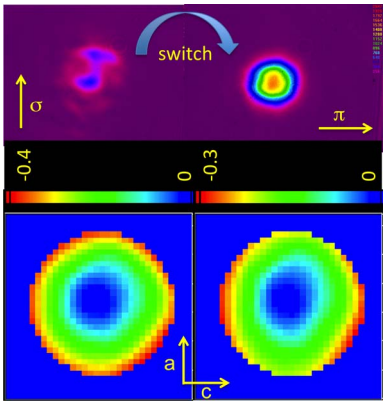

Fig. 5. Evolution of the laser-beam profiles (top), before (left), and after (right) the switch and the associated measured wavefront distortion profiles (bottom). The mask of analysis is 870 μm in diameter.

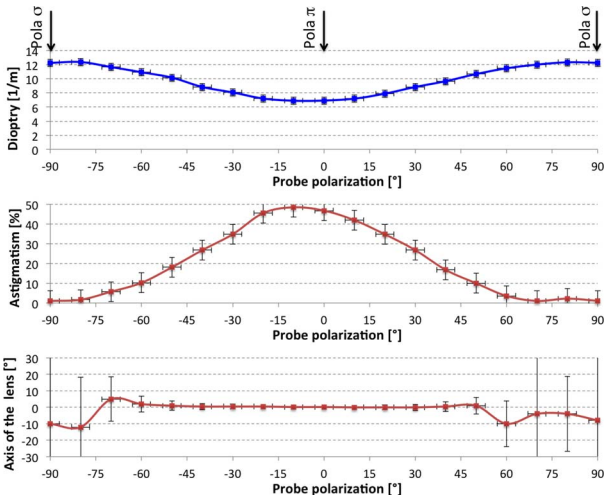

Fig. 6. Thermal lens nature in CALGO versus the laser-beam polarization going through it for 128 W of absorbed power. (Top) Optical dioptry of the lens. (Middle) Astigmatism of the lens. (Bottom) Eigen axis of this lens.

the crystallographic axes ($\vec{a}$ and $\vec{c}$), as shown in Fig. 6 (bottom).

The thermo-optic tensor—deduced from the dioptric power measurements (Fig. 4)—can be defined for the two polarizations, σ and π, and for the two eigen axes of the cylindrical lens, $\vec{a}$ and $\vec{c}$. Equation (1) represents the relations between these coefficients:

$$\chi_{\sigma\vec{c}} = \chi_{\sigma\vec{a}}, \qquad \chi_{\pi\vec{a}} = 0.46\chi_{\sigma\vec{a}}, \qquad \chi_{\pi\vec{c}} = 0.74\chi_{\sigma\vec{a}}. \tag{1}$$

The $\chi_{\sigma\vec{a}}$ coefficient has been calculated measuring the thermal dioptry versus the absorbed power and then determining the sensitivity factor M [17]. This purely linear curve has a sensitivity factor $M = 0.1\ \mathrm{m^{-1}\,W^{-1}}$, which leads to a value for $\chi_{\sigma\vec{a}}$ of $13 \times 10^{-6}\ \mathrm{K^{-1}}$, assuming a fractional thermal load of 5.5% [10].

Taking into account these tensor values, when the switch occurs, the thermal optical dioptry significantly decreases by a factor 1.8, and the astigmatism increases from 1% to 48% (0% corresponding to pure spherical lens and 100% to pure cylindrical lens). This clearly explains the *magic* switching. Actually, when the thermal lens is strong enough to destabilize the σ polarization laser, counteracting, then, the gain difference between σ and π, the laser beam switches to π polarization. The laser beam then observes an important thermal dioptry reduction, enough to get back to a stable region for $\mathrm{TEM_{00}}$. Afterward, the slope of the dioptry versus the power also changes. This last point allows keeping this nice mode even at higher power. Nevertheless, since astigmatism appears, the beam shrinks in its horizontal direction//$\vec{c}$—the direction where the cylindrical lens is the strongest—and a $\mathrm{TEM_{20}}$ spatial mode starts to appear.

In conclusion, an original stabilization process of the spatial mode, including a polarization state change, has been demonstrated for a high-power diode-pumped cw Yb:CALGO laser. This polarization switch occurs, on the one hand, thanks to the particular spectroscopic properties of the Yb:CALGO which, for some cases, can allow relatively easily the switch in polarization

between the two axes of this uniaxial crystal, and, on the other hand, thanks to a strong polarization dependence of the anisotropic thermo-optic coefficient. Actually, a complete study of the thermo-optic coefficient indicated the strange behavior of the thermal lens, which can explain important differences function of the laser-beam polarization propagating in the crystal. This strong impact has been highlighted for the first time—to our best knowledge—in CALGO. This magic mode switching is then very particular and mostly linked to the atypical spectral and thermal properties of the Yb:CALGO. This work may help to optimize future designs of very high-power Yb:CALGO lasers.

This work has been partially supported by the DGA under the founding REI NewMat, by the French National Research Agency (ANR) through the Femtocryble program, and by the network CMDO+ from the CNRS.

References

1. Y. Zaouter, J. Didierjean, F. Balembois, G. Lucas Leclin, F. Druon, P. Georges, J. Petit, P. Goldner, and B. Viana, Opt. Lett. **31**, 119 (2006).
2. A. Agnesi, A. Greborio, F. Pirzio, G. Reali, J. Aus der Au, and A. Guandalini, Opt. Express **20**, 10077 (2012).
3. A. Agnesi, A. Greborio, F. Pirzio, E. Ugolotti, G. Reali, A. Guandalini, and J. Aus der Au, J. Opt. Soc. Am. B **30**, 1513 (2013).
4. J. Boudeile, F. Druon, M. Hanna, P. Georges, Y. Zaouter, E. Cormier, J. Petit, P. Goldner, and B. Viana, Opt. Lett. **32**, 1962 (2007).
5. D. N. Papadopoulos, F. Druon, J. Boudeile, I. Martial, M. Hanna, P. Georges, P. O. Petit, P. Goldner, and B. Viana, Opt. Lett. **34**, 196 (2009).
6. A. Guandalini, G. Greborio, and J. Aus der Au, Proc. SPIE **8235**, 823511 (2012).
7. S. Ricaud, A. Jaffres, P. Loiseau, B. Viana, B. Weichelt, M. Abdou-Ahmed, A. Voss, T. Graf, D. Rytz, M. Delaigue, E. Mottay, P. Georges, and F. Druon, Opt. Lett. **36**, 4134 (2011).
8. K. Beil, B. Deppe, and C. Kränkel, Opt. Lett. **38**, 1966 (2013).
9. S. Ricaud, A. Jaffres, K. Wentsch, A. Suganuma, B. Viana, P. Loiseau, B. Weichelt, M. Abdou-Ahmed, A. Voss, T. Graf, D. Rytz, C. Hönninger, E. Mottay, P. Georges, and F. Druon, Opt. Lett. **37**, 3984 (2012).
10. S. Chénais, F. Balembois, F. Druon, G. Lucas-Leclin, and P. Georges, IEEE J. Quantum Electron. **40**, 1235 (2004).
11. J. Boudeile, J. Didierjean, F. Balembois, F. P. Druon, P. Georges, J. Petit, P. Goldner, and B. Viana, "High power diode pumped Yb^{3+}:$CaGdAlO_4$ laser," in *Advanced Solid-State Photonics*, OSA Technical Digest Series (CD) (Optical Society of America, 2008), paper WE28.
12. S. Chénais, F. Druon, S. Forget, F. Balembois, and P. Georges, Prog. Quantum Electron. **30**, 89 (2006).
13. S. Chénais, F. Balembois, F. Druon, G. Lucas-Leclin, and P. Georges, IEEE J. Quantum Electron. **40**, 1217 (2004).
14. G. Ghosh, *Handbook of Thermo-Optic Coefficients of Optical Materials with Applications* (Academic, 1998).
15. P. Loiko, V. Filippov, K. Yumashev, N. Kuleshov, and A. Pavlyuk, Appl. Opt. **51**, 2951 (2012).
16. S. Biswal, S. O'Connor, and S. Bowman, Appl. Opt. **44**, 3093 (2005).
17. P. Loiko, K. Yumashev, V. Matrosov, and N. Kuleshov, Appl. Opt. **52**, 698 (2013).